Source parameters of earthquakes recorded near the Itoiz dam (Northern Spain)

A. Jiménez[1], J. M. García-García[2,3], M. D. Romacho[2,3], A. García-Jerez[2,3] and F. Luzón[2,3]

[1] School of Environmental Sciences, University of Ulster, Cromore Rd, Coleraine, BT52 1SA, Northern Ireland. a.jimenez@ulster.ac.uk

[2]Department of Chemistry and Physics, University of Almería, Carretera de Sacramento s/n, Cañada de San Urbano, 04120, Almería, Spain.

[3]Instituto Andaluz de Geofísica, Spain.

Abstract

We calculate the source parameters and attenuation from earthquakes recorded near the Itoiz dam, from 2004 to 2009, with magnitudes ranging between 1.2 and 5.2. We use a Genetic Algorithm in order to fit the three-component P-wave spectra with the spectral level, corner frequency and attenuation factor as searching parameters. The obtained moments range from $1.72 \cdot 10^{11}$ to $2.65 \cdot 10^{15}$ Nm, the radii span from 0.09 to 1.00 km, and the stress drops vary from 0.006 to 29.462 MPa. The maximum value for the Q attenuation factor is 794, and the minimum value is 53. We find a good agreement between empirical and theoretical relationship between moment and magnitude. There seems to be a breakdown of self-similarity, but it could be due to the method used. We group the data by means of a Self-Organizing Map and the clusters found are related by their magnitude, and not other considerations.

This is a post-peer-review, pre-copyedit version of an article published in Pure and Applied Geophysics. The final authenticated version is available online at: http://dx.doi.org/10.1007/s00024-014-0883-y

Key words: Source parameters, Reservoir induced seismicity, Genetic Algorithm, Self-Organizing Maps.

1. INTRODUCTION

The Itoiz dam is located in the Jaca-Pamplona basin, in the framework of the South Pyrenean Zone (Fig. 1). On September 18, 2004, a 4.6 mbLg earthquake was widely felt in the region around Pamplona, at the western Pyrenees. Preliminary locations reported an epicenter less than 20 km ESE of Pamplona and close to the Itoiz reservoir, which started impounding in January 2004. This earthquake produced a considerable social alarm about the seismic hazard in the region induced by the impoundment of the reservoir. Our goal is to better understand the mechanisms of the seismicity around the Itoiz dam, and give some insight about its origin. In order to do so, we compare the seismic parameters in that area with other where no induced seismicity is involved.

The region has been extensively studied since the occurrence of the September 18, 2004 event. For example, Ruiz et al. (2006) analyzed the seismic series corresponding to the 18 September 2004 earthquake; Luzón et al. (2009, 2010) and Durá-Gómez and Talwani (2010) studied the effect of the pore pressure due to the impoundment of the reservoir; Santoyo et al. (2010) calculated the stress produced by the reservoir near Itoiz. They showed that the aftershock sequence was indeed produced by the stress transfer caused by the 18 September 2004 earthquake. Rivas-Medina et al. (2011) calculated the seismic hazard near the Itoiz dam. In a previous work (Jiménez et al., 2009; Jiménez and Luzón, 2011, 2012), we studied the main seismic clusters near the Itoiz dam. We did not find any difference between the 18 September 2004 cluster and the others, except for a higher fractal dimension of the epicentre distribution.

This is a post-peer-review, pre-copyedit version of an article published in Pure and Applied Geophysics. The final authenticated version is available online at: http://dx.doi.org/10.1007/s00024-014-0883-y

After the 18 September 2004 event, new stations have been deployed in order to monitor the seismic activity in the area. Among them, the University of Almería installed 5 broadband stations near the reservoir, in order to study the seismicity around the Itoiz dam from 2008 to 2010. With those data, and the ones obtained from the Instituto Geográfico Nacional (IGN), we analyze the source parameters from 45 events since 2004.

It is usually established that reservoir induced seismicity presents lower stress drops than the tectonic earthquakes (Abercrombie and Leary, 1993). Their compilation study included hydraulic fracturing in Fenton Hill, NM (Fehler and Phillips 1991) and coring induced earthquakes from Manitoba, Canada (Gibowicz et al. 1990). In both studies the stress drops were on average one order of magnitude lower ($\Delta\sigma \leq 10$ MPa) than those of naturally occurring earthquakes. This is still observed when the compilation is corrected to use a consistent method for all analyses using earthquake spectra. More recently Mandal et al. (1998) analyzed a set of M 1.4–4.7 induced earthquakes at the Koyna-Warna reservoirs in India and found shallow earthquakes ($1 \leq z \leq 4$ km) with very low stress drops, $\Delta\sigma \leq 2$ MPa. However, some works do not find any difference between natural and induced events (Tomic et al., 2009).

Other interesting question is the breakdown of self-similarity in small earthquakes. For large earthquakes, it is established that the stress drop is constant with the moment, but previous investigations found that the corner frequency of small events increases very slowly or becomes constant with decreasing seismic moment below a certain value, implying a breakdown in the self-similarity of the rupture processes for small earthquakes (Jin et al., 2000). Analyzing earthquakes of magnitude in the range 2.5–7, Atkinson (1993, 2004) noted that the stress drop increases with magnitude (from about 0.3 to 10 MPa) until $M = 4$, above which it appears to have a relatively constant value in the range 10–20 MPa. Atkinson concluded that the low stress drops for small events really reflect low high-frequency spectral

This is a post-peer-review, pre-copyedit version of an article published in Pure and Applied Geophysics. The final authenticated version is available online at: http://dx.doi.org/10.1007/s00024-014-0883-y

amplitudes and not a bandwidth limitation. Other studies, using borehole data, revealed that the apparent corner frequencies of microearthquakes are significantly higher than those estimated from surface recordings (Hauksson et al., 1987; Abercrombie, 1995). The apparent high-frequency limit to corner frequency observed using seismograms recorded at the surface may be due mainly to high attenuation in the weathered, near-surface material, as concluded by Frankel and Wennerberg (1989) and Abercrombie (1995, 1997), Bindi et al. (2001), among others. If there were a breakdown in similarity, it would mean a minimum size for the source dimension, of around 100 m, in the same way we have a maximum size given by the elastic properties of the lithosphere (Archuleta et al., 1982), so that the rupture process would not be self-similar (Mai and Beroza, 2000; Scholz, 1990).

In the present work, we obtain the source parameters (moment, radius and stress drop) from 45 earthquakes recorded near the Itoiz dam (Northern Spain), by using Genetic Algorithms (GA), following Jiménez et al. (2005). We use three component P- wave records. Then we analyze the results and we compare them with other events occurred in a region (the Granada basin, in Southern Spain) where we are sure that no induced seismicity is involved.

2. DATA SELECTION AND ANALYSIS

The digital data used in this work were recorded by 7 short period (1 Hz) seismic stations and 2 accelerometers (from the Instituto Geográfico Nacional, IGN, Spain), 5 broadband instruments and 4 accelerometers (from our research group). We use the three components from all instruments. The dataset comprises 45 low to moderate local earthquakes recorded by 18 three component seismic stations from 2004 to 2009 in Itoiz zone (Navarra, Spain). In Fig. 2 we show the map with all the events analyzed and the locations of the stations. All stations are located in hard rock. As Steidl et al. (1996) point out, site effects can be present. In the method section we will explain how those effects are treated. In Fig. 3 we show the

This is a post-peer-review, pre-copyedit version of an article published in Pure and Applied Geophysics. The final authenticated version is available online at: http://dx.doi.org/10.1007/s00024-014-0883-y

water level at the Itoiz dam, the number of earthquakes and the magnitudes of the seismicity recorded in the region.

Data set was selected on the basis of a high signal to noise ratio, accurate epicentral location and sufficient separation between P and S phases. The recording affected by saturation effects and other problems were discarded. The body wave magnitude (mbLg) of the selected events, ranged between 1.2 and 5.2.

The location accuracy relied upon a very good reading of the first P-wave arrival and the relative large number of stations used. We used a window length that includes the maximum amplitude of the P-wave and avoids overlapping with other types of waves. Most of the events have depths of less than 10 km (between 1 and 11 km), so they are considered shallow events. The hypocentral distances are between 0.6 km and 174 km. At this distance range, the seismic records are mainly influenced by the near-surface structure of the crust because most source-station ray paths are confined to the crust (Fernández et al., 2010). In Fernández et al. (2010) they speak about a range of distances between 0 and 100 km. For larger distances, the effect of the near mantle can affect the values for the Q factors. However, we are confident that this is the range of most of our distances between source and station. The events are recorder very close to the stations in most of the cases. We only have two stations that are not very close (See Fig. 2). It should be noted that the impulsive P-wave arrival are characteristic to all selected events.

All the spectra studied from P-wave, were calculated using a Fast Fourier Transform. First, the signal was base-line corrected subtracting the average of all points of the record. The time series were windowed from the start of the phase by using a both ends 10 percent cosine taper. The resultant seismogram was padded with zeros to an integer power-of-2 prior to the FFT. Signal windows of varying lengths were tested in order to select a length that would avoid contamination from other phases and maintain the resolution and stability of the

This is a post-peer-review, pre-copyedit version of an article published in Pure and Applied Geophysics. The final authenticated version is available online at: http://dx.doi.org/10.1007/s00024-014-0883-y

spectra (Garcia et al., 1996). The sampling rate is of 200 samples per second for accelerometer recording and of 100 samples per second for velocity recordings. The spectra were subsequently corrected for instrumental response. Preevent noise windows of equal length than the signal window were used to compute the signal noise relation (SNR) and only records with a SNR higher than 3 were retained. Spectral amplitudes were divided by the appropriate power of frequency to give a displacement spectrum. A total of 360 P-wave spectra are used in this study. Figure 1 shows the distribution of the epicentres of the considered earthquakes.

3. METHOD

Following Abercrombie (1995), and after correcting for the geometrical spreading and instrumental response, the problem is solved for the spectral level Ω_0 and the corner frequency f_0, while simultaneously correcting for path-averaged attenuation Q, by fitting P and S-wave spectra with the ω^{-2} source model proposed by Boatwright (1978). The spectral shape is described by:

$$\Omega(f) = \frac{\Omega_0 e^{-\pi f t / Q}}{\left[1 + \left(\frac{f}{f_0}\right)^4\right]^{1/2}} \qquad (1)$$

where Ω_0 is the spectral level, f_0 is the corner frequency, Q is the path-averaged attenuation factor, and t is the travel time. With the values of Ω_0 and f_0, the seismic source parameters can be obtained from the well-known relationships established for a circular fault (Brune, 1970; Brune, 1971; Hanks and Wyss, 1972). Additional information is the knowledge of the attenuation factor Q. It represents the loss of the energy of the waves along

This is a post-peer-review, pre-copyedit version of an article published in Pure and Applied Geophysics. The final authenticated version is available online at: http://dx.doi.org/10.1007/s00024-014-0883-y

the path between the source and the station, and it can give useful information about the structure of the earth (Del Pezzo et al., 1991).

We use a Q independent on the frequency. Fehler and Phillips (1991) demonstrated that variation of *Q* from 600 to 3000 changed the corner frequency by less than 15% from the result obtained by assuming a constant average *Q*. A more complex attenuation function does not result in a better fit to the data, and produces multiple equivalent solutions, in the sense that they have the same fitting accuracy (Jiménez et al., 2005). Among these other functions, we tried to include the kappa factor (García et al., 2004) accounting for the site effect. No improvement was found in using it, and a constant Q was the better choice. So, the Q values account for the attenuation along the path, and the site effect at mid-high frequencies can not be distinguished from the noise. In the aforementioned article (Jiménez et al., 2005), where we used the same method as the one we use here, we calculated the seismic parameters for a set of earthquakes that were the same as the work in (García et al., 1996), where the Snoke's method (Snoke, 1987) was performed. Both methods gave similar results. Thus, we are confident that the method is stable.

We use Genetic Algorithms (GA) in order to fit the three parameters that describe the spectrum. GA are methods of global optimization, which have proven effective when the models are described by a few parameters, the problem is nonlocal (the global optimum is needed, but there are many local optima) and nonlinear, and there is no a priori knowledge of the behavior of the function. In geophysics, and particularly in seismology, many problems often have such features. The basic principles of *GA* were established by Holland (1975), and are well described, for example, in Goldberg (1989), Davis (1991), Michalewicz (1992) or Reeves (1993).

The GA used in this paper has been implemented in Jiménez et al. (2005). The definitive search strategy chosen was selection by rank wheel, crossover based on fitness, and

This is a post-peer-review, pre-copyedit version of an article published in Pure and Applied Geophysics. The final authenticated version is available online at: http://dx.doi.org/10.1007/s00024-014-0883-y

replacement by rank wheel. This strategy is moderately elitist, because the best individuals are easily selected, but there is low selection pressure. The simple GA was improved with the reinitialization of the population when the convergence stays blocked (Jiménez et al., 2005).

The algorithm was tested with synthetic data and applied to the spectra of 13 earthquakes in Granada (Southern Spain). The obtained parameters are the corner frequency, the spectral level and the attenuation along the path. Hough et al. (1989) showed that the trade-off between *Q* and the corner frequency is strong when a wide range of values for both parameters are used to fit the data. So then it is important to use a good optimization tool to calculate those parameters. That's the reason of using a powerful tool such as a GA. In Jiménez et al. (2005) we compared the implemented GA with the commonly used Nelder–Meade algorithm (Tomic et al., 2009), and found that our technique is more appropriate for this task. For further details, see Jiménez et al. (2005).

For obtaining the source parameters, the best fit was chosen for introducing its spectral parameters to the relationships given by Brune (1970) and Hanks and Wyss (1972):

$$M_0 = \frac{4\pi\rho v^3 \Omega_0 d}{KR} \quad (2)$$

$$r = \frac{kv}{f_c} \quad (3)$$

$$\Delta\sigma = \frac{7M_0}{16r^3} \quad (4)$$

being ρ the density of the medium (2.7 gm/cm^3), *v* the velocity (5.5 km/s for the P-wave, following Ruiz et al. (2006)), *d* being the hypocentral distance, accounting for the geometrical spreading; *K* being the wave amplification at the free surface; *R* being the radiation pattern coefficient for the P and S- waves. Since the focal mechanism could not be determined (the spectra correspond to small earthquakes), the rms averages *R(P)=0.52* and

This is a post-peer-review, pre-copyedit version of an article published in Pure and Applied Geophysics. The final authenticated version is available online at: http://dx.doi.org/10.1007/s00024-014-0883-y

R(S)=0.63 were used (Aki and Richards, 1980); *k* is a factor that depends on the model. If we use Brune's model, this factor is 0.372, but if we use Madariaga's model (Madariaga, 1976), it is 0.21. So, the radii are 1.76 times larger for Brune (1970) model, and the stress drop is 5.6 times larger for the Madariaga (1976) model. The Sato and Hirasawa (1973) model lies in between. All three models are in common usage, and the model used must be considered when comparing results from different Studies (Tomic et al., 2009).

In order to remove the effect of the free surface in a three component record, we follow the method described in Shieh (1995). The motion of the particle we have in the record of the window where we suppose the P wave is the composition of the incident P-wave, the reflected and the SV-wave produced by the P incident. So, by means of the equations in Aki and Richards (1980), we have the horizontal and vertical components of the motion. By dividing the horizontal into the vertical component of the records, and comparing this quantity to the theoretical one, we can calculate the angle of incidence, and then remove the free surface effect (Shieh, 1995). In that way, we can calculate the spectrum of the incident P-wave. So, we first calculate the spectrum with the free surface effect removed and then fit the spectrum with the GA to obtain the source parameters. This is a very important step, since we only want the contribution of the P wave, and not that of the SV-wave, that contaminates the spectrum. We performed the same transformation for S-waves, but the separation of the SV and SH waves was very problematic, so that they were highly contaminated by other phases. Thus, we only used the P-wave for our calculations.

Each real spectrum was introduced in the GA implemented, with the following considerations for the fitting parameters: first, the spectral level limits for the search in that parameter were obtained by visualizing the spectrum. Although the source spectrum computed from numerical data might present large uncertainties, we gave a wide range for the searching limits for the spectral level (1 or 2 orders of magnitude, depending on the

This is a post-peer-review, pre-copyedit version of an article published in Pure and Applied Geophysics. The final authenticated version is available online at: http://dx.doi.org/10.1007/s00024-014-0883-y

spectrum); second, the corner frequency were searched between 0.1 and 25 Hz, a reasonable value for the magnitudes involved; and finally, a maximum of 800 was introduced for the *Q* values, after consulting several studies made in the zone (Pujades et al., 1990; González, 2001). The resolution for each parameter (spectral level, corner frequency and Q factor) was of 5, 6, and 7 bits, respectively. That is, 2 to the power of 5, 6 and 7. The population (number of models in each generation) and number of generations were 20 and 100, respectively. The algorithm was executed three times, and the best fit was selected for calculating the source parameters. We found that with three times only we obtained consistent results, so we did not increase the number of runs, and therefore the computation time.

For each event, the average values for seismic moment, source radius and stress drop were computed. Calculations were made using three component P-wave records. The average values were estimated as (Archuleta et al., 1982):

$$\bar{x} = antilog10\left(\frac{1}{N}\sum_{i=1}^{N} log10x_i\right) \qquad (5)$$

where N is the number of stations used. The reason is that the errors associated with Ω_0 and r are log-normally distributed. The standard deviation of the logarithm, $SD(\log\bar{x})$ was estimated by calculating the variance of the individual logarithms about the mean logarithm:

$$SD\left(log10\bar{x}\right) = \left(\frac{1}{N-1}\sum_{i}^{N}\left[log10x_i - log10\bar{x}\right]^2\right)^{1/2} \qquad (6)$$

and multiplicative error factors, *Ex*, were calculated as:

$$Ex = anti\log10(SD(\log10x)) \qquad (7)$$

This is a post-peer-review, pre-copyedit version of an article published in Pure and Applied Geophysics. The final authenticated version is available online at: http://dx.doi.org/10.1007/s00024-014-0883-y

4. RESULTS AND DISCUSSION

In Fig. 4 we show an example of fitted spectrum. All the spectra had good visual correspondence between the fitted line and the experimental data. In Table 1 we write the results for the source parameters of all the events, with their corresponding multiplicative errors, when possible (when more than two stations recorded the earthquake). The higher errors correspond to the stress drops, because they are a derived quantity, calculated from the moment and radius. The averaged error for the moment is 2.5, and for the radius is 1.83, which are very good. Note that the smallest error in logartimic scale is 1, which means that all the results were the same. The corner frequencies span from 1.66 to 23.44Hz. So, the sampling rate of 100 and 200 samples/sec are appropriate for the studied data set. Note that we use Brune's model, the P-wave velocity is set at 5.5 km/s, and the minimum source radius is 0.09 km.

The obtained moments range from $1.72 \cdot 10^{11}$ to $2.65 \cdot 10^{15}$ Nm, with an average value of $8.51 \cdot 10^{13}$ Nm; the radii span from 0.09 to 1.00 km, with an average value of 0.32 km. Finally, the stress drops vary from 0.006 to 29.462 MPa, with an average value of 1.076 MPa.

The values we find are very similar to the ones obtained by Tusa and Gresta (2008) in southern Sicilia, with tectonic events, and magnitudes ranging from 0.7 to 4.6. The stress drops found by Prejean and Ellsworth (2001) in the Long Valley Caldera, Eastern California, range from 0.01 to 30 MPa, with magnitudes spanning from 0.5 to 5, a result which is very similar to the one obtained in the present study.

As we mentioned before, Mandal et al. (1998) analyzed a set of M 1.4–4.7 induced earthquakes at the Koyna-Warna reservoirs in India and found shallow earthquakes ($1 \leq z \leq 4$ km) with very low stress drops, $\Delta\sigma \leq 2$ MPa. The depths of the events in our data set vary from 0 to 11.1 km, so they are shallow earthquakes too. In Table 1 we can observe that 96%

This is a post-peer-review, pre-copyedit version of an article published in Pure and Applied Geophysics. The final authenticated version is available online at: http://dx.doi.org/10.1007/s00024-014-0883-y

of the events have stress drops lower than 2 MPa, if we use the Brune (1970) model, and 80% are lower than 2 MPa if we use the Madariaga (1976) model. In Tomic et al. (2009) they find higher stress drops, because they use the Madariaga (1976) model. For events with magnitude ranging from 0.3 to 3.1, Hua et al. (2013) found very low values for the static stress drops (from 0.01 to 0.26 MPa). It has to be noted that the highest stress drop is found for the 5.2 event, and it is much higher than the stress drops found for the other earthquakes (29.462 MPa for the 5.2 earthquake, and 96% of events are below 2 MPa). As can be seen in Table 1, the multiplicative error factors for the 5.2 events are low (2.19, 1.48, 1.54, for the moment, radius and stress drop), so we are confident that the high value for its stress drop is accurate.

Now we will analyze the results obtained for the attenuation factors. It is important to remember that we obtain the Q factors for each path, in order to compare our results with other attenuation studies done in the area of interest. In Fig. 5 we show the Q factors in function of the distance. Note that the Q factor is calculated for each path, so no error can be associated. As stated before, each fitted spectrum is the result of three calculations of the parameters with the GA, so that the obtained parameters are very stable. The maximum value is 794, and the minimum value is 53, with an average value of 444. This means that the limits imposed in the search (between 10 and 800) were reasonable, and in agreement with previous studies in the region (Pujades et al., 1990; González, 2001). We find that, in general, the attenuation factor increases up to an epicentral distance of around 50 km, indicating that the scattering of the waves reaches the Moho, which is very deep in this area: around 46-48 km (Pedreira et al., 2003).

Pujades et al. (1990), and more recently González (2001), calculated the Q-coda values for this region. The latter obtained Q_0=53 and ν=1.12 for the ELIZ station (from the IGN), the closest to our area of study, assuming a relationship between Q and the frequency given by:

This is a post-peer-review, pre-copyedit version of an article published in Pure and Applied Geophysics. The final authenticated version is available online at: http://dx.doi.org/10.1007/s00024-014-0883-y

$$Q = Q_0\left(\frac{f}{f_0}\right)^{\nu} \quad (8)$$

If we use the averaged value of 444 (the average value we obtained) for all the frequencies, and assuming the same ν, we would obtain Q_0=26, also very low. Note that our distances are lower (they use data up to 300 km), and so the value for the attenuation should be lower too (Zelt et al., 1999). If we suppose an exponent ν=0.85, close to the value of the EGRA station, also used for studying the attenuation in the Pyrenees by González (2001), the value for Q_0 would be 53. So that would be the range of parameters for the attenuation we found, in good agreement with the studies in the region. In any case, as González (2001) says, the relationship in Eq. (8) does not hold for a long range of frequencies, as we used in our calculations. Also, note that we use a constant value for all the frequencies, so the comparisons have to be taken carefully.

Now we are analyzing the relationship between the different magnitudes calculated. In first place, in Fig. 6 we plot the moment versus the magnitude of the events. The best fit for the line is $M_L = (0.66 \pm 0.05)\log M_0 - (5.9 \pm 0.7)$, with correlation coefficient of 0.88. This relationship is exactly the one expected theoretically (M_L=2/3 log M_0 - 6) if the moment is expressed in Nm, as we have done (Deichmann, 2006). The significance of the obtained relationship is of 5.89σ. This means that our calculation for the seismic moment is theoretically consistent with the magnitude given by the IGN.

In order to test the hypothesis of constant stress drop, in Fig. 7 we show the relationship between source radius and seismic moment. The lines represent the contours with constant stress drops. As we can see, the stress drops vary, and have a high dispersion in their values. It is a similar result to the one obtained by Tusa and Gresta (2008). We did not find a relationship between corner frequency and moment either. There is a trend of increasing moment with decreasing corner frequency, but the correlation coefficient is very low. Note

This is a post-peer-review, pre-copyedit version of an article published in Pure and Applied Geophysics. The final authenticated version is available online at: http://dx.doi.org/10.1007/s00024-014-0883-y

that the errors in the source radii are low (around 1 or 2 in Table 1), which means that the corner frequencies have been correctly calculated. The large errors in the stress drops are a consequence of being a parameter calculated from both moment and radius, with their associated errors.

In Fig. 8 we see that the stress drop increases with increasing moment. The best fit gives $\log\Delta\sigma = (0.81 \pm 0.08)\log M_0 - (5.4 \pm 1.1)$ with a correlation coefficient of 0.77, and a significance of 6.4σ. We did not use the data with no error in the fit, because they were recorded only in 1 or 2 stations. The trend with respect to the magnitude is also positive, as Jost et al. (1998) found in injection-induced earthquakes of magnitude ranging between -2 and 0. Oncescu at al. (1994), Haar et al. (1984) and Hua et al. (2012, 2013) found that stress drop increases with moment too.

In our data, a trend of increasing stress drop with increasing seismic moment is evident, suggesting a self-similarity violation. The breakdown in similarity that we observe is very similar to that Atkinson (1993, 2004) found in northeastern America for events having Mw less than about 4, and Tusa and Gesta (2008), with earthquakes in southern Sicilia. However, Castro et al. (1995), for earthquakes with magnitude between 2.8 and 4.8 found that the stress drop decreases with increasing moment. Drouet et al. (2005) found that constant stress drop is valid for the Pyrenees in the range of magnitude 2.7-5.4, which is the opposite we found. Drouet et al. (2008) found a slight tendency to higher stress drops for higher moments in the Western Pyrenees, but they interpreted it as an effect of the finite-frequency bandwidth that they analyzed. Mori and Frankel (1990) and Smith and Priestly (1993) say that there is no apparent correlation between stress drop with moment neither with depth. We did not find any relationship between stress drop and depth, in agreement with the results in Moya et al. (2000), with events of magnitude between 3.3 and 4.9.

This is a post-peer-review, pre-copyedit version of an article published in Pure and Applied Geophysics. The final authenticated version is available online at: http://dx.doi.org/10.1007/s00024-014-0883-y

Ide et al. (2003) think that the use of constant Q and/or propagation effects can introduce artificial size dependence in apparent stress measurements. They use data from boreholes, and can calculate Empirical Green Functions to correct by path and site effects. We do not have borehole data, and we can not calculate appropriate Empirical Green Functions, because most of the event have a low magnitude, so we can not use their method in order to compare the results with our assumption of constant Q.

Now we will compare our results near the Itoiz dam with other obtained in the Granada basin, where we know that there is not reservoir induced seismicity. The source parameters were analyzed in García et al. (1996), with earthquakes of magnitudes ranging from 1 to 3.5. We will classify the data into clusters, for both regions, the Itoiz dam and the Granada basin, by means of Self-Organizing Maps (SOM), and then we will compare the two results.

The SOM algorithm is a convenient, unsupervised learning method, which is widespread in various scientific fields (see references in Kohonen (2001)). They provide a way of representing multidimensional data in much lower dimensional spaces - usually one or two dimensions. This process, of reducing the dimensionality of vectors, is essentially a data compression technique known as *vector quantisation*. In addition, the Kohonen technique creates a network that stores information in such a way that any topological relationships within the training set are maintained. One of the most interesting aspects of SOM is that they learn to classify data *without supervision*. The way SOM go about reducing dimensions is by producing a map of usually 1 or 2 dimensions which plot the similarities of the data by grouping similar data items together. So SOM accomplish two things, they reduce dimensions and display similarities.

SOM have already been applied, in different contexts, for active seismic data sets (Essenreiter et al. 2001; Klose 2006; De Matos et al. 2007; Higgins et al., 2011) and in seismology (Maurer et al. 1992; Musil & Plešinger 1996; Tarvainen 1999; Plešinger et al.

This is a post-peer-review, pre-copyedit version of an article published in Pure and Applied Geophysics. The final authenticated version is available online at: http://dx.doi.org/10.1007/s00024-014-0883-y

2000; Allamehzadeh and Mokhtari, 2003; Ozerdem et al. 2006; Esposito et al. 2008; Carniel et al., 2009; Köhler et al. 2009, 2010). We will use them as a classification tool where the variables are the moment and the stress drop. We use the MATLAB functions for obtaining our clusters. The variables are the logarithm of the moment and the stress drop, divided by the sum of the logarithms in each case. In Fig. 9-10 we can see the obtained clusters. Each node represents a cluster found by the algorithm. The lines represent the nearest nodes in the clustering algorithm. We observe that the clusters are ordered by magnitude (and not by other factors such as location or time) with increasing stress drop when moment increases. It is in agreement to the previous results for the relationship between moment and stress drop. So there seems to be a clustering of the events depending on the magnitude only, for both regions. This dependence on the magnitude only for the Itoiz region was also found in Jiménez and Luzón (2011), where we analyzed the seismicity near the Itoiz dam by means of weighted complex networks. This comparison is interesting because we are analyzing two different kind of seismic sets, with supposedly different seismicity origin. SOM are classifiers that are not influenced by a priori knowledge of the data. So, the fact that both regions present the same behaviour with respect to the relationship between stress drops and moments is very important. It is also very interesting to see that time does not influence the relationship between moment and the stress drop in the data, something that could indicate an effect of the redistribution of stresses with time near the Itoiz dam, due to the impoundment of the reservoir.

In Fig. 11 we show the data from García et al. (1996). There we see an increase of the stress drop with increasing magnitude, as we found in the present work.

This is a post-peer-review, pre-copyedit version of an article published in Pure and Applied Geophysics. The final authenticated version is available online at: http://dx.doi.org/10.1007/s00024-014-0883-y

5. CONCLUSIONS

We have analyzed the seismicity near the Itoiz dam, by calculating the source parameters and attenuation from earthquakes recorded from 2004 to 2009, with magnitudes between 1.2 and 5.2. We assume a Boatwright (1978) model for the source, and a spectral falloff with *Q* not dependent on the frequency for the attenuation. The parameters to be found by the GA are the spectral level, the corner frequency, and the attenuation factor (Jiménez et al., 2005). With those data, we calculate the source parameters following Brune (1970, 1971). The obtained moments range from $1.72 \cdot 10^{11}$ to $2.65 \cdot 10^{15}$ Nm, the radii span from 0.09 to 1.00 km, and the stress drops vary from 0.006 to 29.462 MPa. The maximum value for the Q attenuation factor is 794, and the minimum value is 53. The values we find are very similar to the ones obtained by Tusa and Gresta (2008) in southern Sicilia, with tectonic events, and the stress drops are not particularly low, as some authors think it is supposed for fluid-injection induced seismicity. The classification by means of SOM gives us clusters that depend on the magnitude, and not other considerations, in agreement with the results in Jiménez et al. (2011). It is remarkable the coincidence between the theoretical and empirical relationship between the obtained moments and the magnitude. We found an increase of the stress drop with increasing moment with high significance, which is a breakdown of the self-similarity in the process. As Ide et al. (2003) point out, the use of constant Q and/or propagation effects can introduce artificial size dependence in apparent stress measurements.

Acknowledgments

We wish to thank the Confederación Hidrográfica del Ebro (CHE) for allowing us to use their facilities and their seismic data. We also thank the Instituto Geográfico Nacional (IGN), Spain. This work was partially supported by the Secretaría General para el Territorio y la

This is a post-peer-review, pre-copyedit version of an article published in Pure and Applied Geophysics. The final authenticated version is available online at: http://dx.doi.org/10.1007/s00024-014-0883-y

Biodiversidad part of the Ministerio de Medio Ambiente, Rural y Marino, Spain, under grant 115/SGTB/2007/8.1, by EU with FEDER and by the research team RNM-194 of the Junta de Andalucía, Spain. The work of AJ is supported by a Juan de la Cierva grant, from the Spanish Government.

References

Abercrombie, R. E. (1995), Earthquake source scaling relationships from 1 to 5 *M*L using seismograms recorded at 2.5 km. depth, *J. Geophys.Res.* 100**,** 24015–24036.

Abercrombie, R. E. (1997), Near surface attenuation and site effects from comparison of surface and deep borehole recordings, *Bull. Seism. Soc.Am.* 87**,** 731–744.

Abercrombie, R.E. and Leary, P. (1993), Source parameters of small earthquakes recorded at 2.5 km depth, Cajon Pass, Southern California: implications for earthquake scaling, *Geophys. Res. Lett.,* 20**,** 1511–1514.

Aki, K. and Richards, P. G. (1980), *Quantitative seismology*, W. H. Freeman, San Francisco.

Allamehzadeh, M. and Mokhtari, M. (2003), Prediction of Aftershocks Distribution Using Self- Organizing Feature Maps (SOFM) and Its Application on the Birjand-Ghaen and Izmit Earthquakes. *JSEE: Fall 2003*, 5(3), 1-15.

Archuleta, R., Cranswick, E., Mueller, C. and Spudich, P. (1982), Source parameters of the 1980 Mammoth Lakes, California, earthquake sequence, *J. Geophys. Res.* 87**,** 4595–4607.

Atkinson, M. G. (1993), Earthquake source spectra in eastern north America, *Bull. Seism. Soc. Am.*, 83, 1778–1798

This is a post-peer-review, pre-copyedit version of an article published in Pure and Applied Geophysics. The final authenticated version is available online at: http://dx.doi.org/10.1007/s00024-014-0883-y

Atkinson, M. G. (2004), Empirical attenuation of ground-motion spectral amplitudes in southeastern Canada and the northeastern United States, *Bull. Seism. Soc. Am*. 94, 1079–1095.

Bindi, D., Spallarossa, D., Augliera, P. and Cattaneo, M. (2001), Source parameters from the aftershocks of the 1997 Umbria - Marche (Italy) seismic sequence. *Bull. Seism. Soc. Am*., 91, 448–455.

Boatwright, J. (1978), Detailed spectral analysis of two small New York state earthquakes, *Bull. Seism. Soc. Am.* 68**,** 1117–1131.

Brune, J. N. (1970), Tectonic stress and the spectra of seismic shear waves from earthquakes, *J. Geophys. Res.* 75**,** 4997–5009.

Brune, J. N. (1971), Correction to Tectonic stress and the spectra of seismic shear waves from earthquakes by J. N. Brune, *J. Geophys. Res.*, 76**,** 5002.

Carniel, R. Barbui, L. and Malisan, P. (2009), Improvement of HVSR technique by self-organizing map (SOM) analysis, Soil Dynamics and Earthquake Engineering, 29 (6), 1097-1101, doi:10.1016/j.soildyn.2008.11.008.

Castro, R.R., Munguía, L. and Brune, J.N. (1995), Source spectra and site response from P and S waves of local earthquakes in the Oaxaca, México subduction zone. *Bull. Seism. Soc. Am*, 85, 923-936.

Davis, L. (*ed.*) (1991). Handbook of Genetic Algorithms, *Van Nostrand Reinhold, New York*.

De Matos, M., Osorio, P. and Johann, P. (2007), Unsupervised seismic facies analysis using wavelet transform and self-organizing maps, *Geophysics*, 72**,** 9–21. doi: 10.1190/1.2392789.

This is a post-peer-review, pre-copyedit version of an article published in Pure and Applied Geophysics. The final authenticated version is available online at: http://dx.doi.org/10.1007/s00024-014-0883-y

Del Pezzo, E., de Martino, S., de Miguel, F., Ibáñez, J. M. and Sorgente, S. (1991), Characteristics of the seismic attenuation in two tectonically active zones of Southern Europe, *Pure Appl. Geophys.,* 135**,** 91–106.

Deichmann, N. (2006), Local Magnitude, a Moment Revisited, Bull. Seism. Soc. Am., 96 (4), 1267–1277, doi: 10.1785/0120050115.

Drouet, S., Souriau, A., and Cotton, F. (2005), Attenuation, seismic moment, and site effects for weak-motion events: application to the Pyrenees, *Bull. Seism. Soc. Am.*, 95 (5), 1731–1748. doi: 10.1785/0120040105.

Drouet, S., Chevrot, S., Cotton, F., and Souriau, A. (2008), Simultaneous inversion of source spectra, attenuation parameters, and site responses: application to the data of the French Accelerometric Network, *Bull. Seism. Soc. Am*. 98, 198-219.

Durá-Gómez, I. and Talwani, P., (2010), Reservoir-induced seismicity associated with the Itoiz Reservoir, Spain: a case study, *Geophys. J. Int*., 181, 343–356, 2010, doi: 10.1111/j.1365-246X.2009.04462.x.

Esposito, A., Giudicepietro, F., D'Auria, L., Scarpetta, S., Martini, M. Coltelli, M. and Marinaro, M. (2008), Unsupervised neural analysis of very-long-period events at Stromboli volcano using the self-organizing maps, *Bull. Seism. Soc. Am.,* 98(5), 2449–2459, doi: 10.1785/0120070110.

Essenreiter, R., Karrenbach M. and Treitel, S. (2001), Identification and classification of multiple reflections with self-organizing maps, *Geophys.Prospect.,* 49(3), 341–352, doi: 10.1046/j.1365-2478.2001.00261.x.

Fehler, M., and Phillips, W.S. (1991), Simultaneous inversion for *Q* and source parameters of microearthquakes accompanying hydraulic fracturing in granitic rock, *Bull. seism. Soc. Am*, 81**,** 553–575.

This is a post-peer-review, pre-copyedit version of an article published in Pure and Applied Geophysics. The final authenticated version is available online at: http://dx.doi.org/10.1007/s00024-014-0883-y

Fernández, I., Castro, R. and Huerta, C. (2010), The spectral decay parameter kappa in Northeastern Sonora, Mexico, *Bull. Seism. Soc. Am.*, 100 (1), 196-206, doi:10.1785/0120090049.

Frankel, A., and Wennerberg, L. (1989), Microearthquake spectra from the Anza, alifornia, seismic network: site response and source scaling, *Bull. Seism. Soc. Am.* 79**,** 581–609.

García García, J. M., Romacho M. D. and Jiménez, A. (2004), Determination of near-surface attenuation, with κ parameter, to obtain the seismic moment, stress drop, source dimension and seismic energy for microearthquakes in the Granada Basin (Southern Spain), *Phys. Earth Planet. Int.* 141, 9-26.

García, J. M., Vidal, F., Romacho, M. D., Martín-Marfil, J. M., Posadas, A. and Luzón, F. (1996), Seismic source parameters for microearthquakes of the Granada basin (southern Spain), *Tectonophysics*, 261**,** 51–66.

Gibowicz, S. J., Harjes, H. P., and Shäfer, M. (1990), Source parameters of seismic events at Heinrich Robert mine, Ruhr basin, Federal Republic of Germany: evidence for non double-couple events, *Bull. Seism. Soc. Am.* 80**,** 1157–1182.

Goldberg, D. E. (1989). Genetic Algorithms, *in Search, Optimization and Machine Learning, Addison-Wesley, Reading, MA.*

González, J. (2001), Estructura anelástica de coda-Q en la Península Ibérica, PhD Thesis, Departament d'Enginyeria del Terreny, Cartogràfica i Geofísica Universitat Politècnica de Catalunya.

Haar, L.C., Fletcher, J.B., and Mueller, C.S. (1984), The 1982 Enola, Arkansas, swarm and scaling of ground motion in the eastern United States. *Bull. Seism. Soc. Am.*, 74, 2463–2482.

This is a post-peer-review, pre-copyedit version of an article published in Pure and Applied Geophysics. The final authenticated version is available online at: http://dx.doi.org/10.1007/s00024-014-0883-y

Hanks, Th. C., and Wyss, M. (1972), The use of body-wave spectra in the determination of seismic-source parameters, *Bull. Seism. Soc. Am.* 62**,** 561–589.

Hauksson, E., Teng, T. and Henyey, T. L. (1987), Results from a 1500 m deep, three-level downhole seismometer array: site response, low *Q* values, and *f*max, *Bull. Seism. Soc. Am.*, 77**,** 1883–1904.

Higgins, M., Ward, C. and De Angelis, S. (2011), Determining an Optimal Seismic Network Configuration Using Self-Organizing Maps, in *Advances in Artificial Intelligence Lecture Notes in Computer Science*,Vol. 6657/2011, 170-173, doi: 10.1007/978-3-642-21043-3_20.

Holland, J. (1975). Adaptation, *in Natural and Artificial Systems, University of Michigan Press, Ann Arbor*.

Hough, S. E., Jacob, K., Busby, R., and Friberg, P. (1989), Ground motion from a magnitude 3.5 earthquake near Massena, New York: evidence for poor resolution of corner frequency for small events, *Seism. Res. Lett.*, 60**,** 95–1000.

Hua, W., Chen, Z., Zheng, S. (2012), Source Parameters and Scaling Relations for Reservoir Induced Seismicity in the Longtan Reservoir Area. *Pure and Applied Geophysics* , 170(5), 767-783.

Hua, W., Zheng, S., Yan, C., Chen, Z. (2013), Attenuation, Site Effects, and Source Parameters in the Three Gorges Reservoir Area, China. *Bulletin of the Seismological Society of America*, 103(1), 371-382.

Ide, S., Beroza, G. C., Prejean, S.G., and Ellsworth, W.L. (2003), Apparent break in earthquake scaling due to path and site effects on deep borehole recordings, *J. Geophys. Res.*, 108**,** B52271, doi:10.1029/2001JB001617.

This is a post-peer-review, pre-copyedit version of an article published in Pure and Applied Geophysics. The final authenticated version is available online at: http://dx.doi.org/10.1007/s00024-014-0883-y

Jiménez, A., García, J. M., and Romacho, M. D., **(**2005), Simultaneous Inversion of Source Parameters and Attenuation Factor Using Genetic Algorithms. *Bull. Seism. Soc. Am*. 94, 1401-1411, doi: 10.1785/0120040116.

Jiménez, A., Tiampo, K. F., Posadas, A. M. and Donner, R. (2009), Analysis of complex networks associated to seismic clusters near the Itoiz reservoir dam. *The European physical journal*. Special topics, 181-195, doi: 10.1140/epjst/e2009-01099-1.

Jiménez, A., and Luzón, F. (2011), Weighted complex networks applied to seismicity: the Itoiz dam (Northern Spain). *Nonlinear Processes in Geophysics*, 18, 477–487, doi:10.5194/npg-18-477-2011.

Jiménez, A. and Luzón, F. (2012), Diffusion Entropy Analysis and Hurst exponent near the Itoiz dam, *in Handbook on the Classification and Application of Fractals, (Nova Science Publishers, Inc* 2012*),* ISBN**:** 978-1-61324-198-1, pp. 115-131.

.Jin, A., Moya, C. A. and Ando, M. (2000), Simultaneous determination of site responses and source parameters of small earthquakes along the Atotsugawa fault zone, central Japan, *Bull. Seism. Soc. Am.,* 90**,** 1430–1445.

Jost, M. L., Büsselberg, T., Jost, O., and Harjes, H.P. (1998), Source parameters of injection-induced microearthquakes at 9 km depth at the KTB deep drilling site, Germany, *Bull. Seism. Soc. Am.,* 88 (3), 815-832.

Klose, C. (2006), Self-organizing maps for geoscientific data analysis: geological interpretation of multidimensional geophysical data, *Comput. Geosci.,* 10(3), 265–277, doi: 10.1007/s10596-006-9022-x.

Kohonen, T. (2001), *Self-Organizing Maps,* Springer Series in Information Sciences, Vol. 30, Third Extended Edition, 501 pp, Springer Berlin, Heidelberg, New York, 1995, 1997, 2001.

This is a post-peer-review, pre-copyedit version of an article published in Pure and Applied Geophysics. The final authenticated version is available online at: http://dx.doi.org/10.1007/s00024-014-0883-y

Köhler, A., Ohrnberger, M., and Scherbaum, F. (2009), Unsupervised feature selection and general pattern discovery using Self-Organizing Maps for gaining insights into the nature of seismic wavefields, *Comput. Geosci.*, **35**(9), 1757–1767, doi:10.1016/j.cageo.2009.02.004.

Köhler, A., Ohrnberger, M. and Scherbaum, F. (2010), Unsupervised Pattern Recognition in Continuous Seismic Wavefield Records using Self-Organizing Maps, *Geophys. J. Int*., 182, 1619-1630. doi: 10.1111/j.1365-246X.2010.04709.x

Luzón, F., García-Jerez, A., Santoyo, M. A., and Sánchez-Sesma, F. J. (2009), A hybrid technique to compute the pore pressure changes due to time varying loads: application to the impounding of the Itoiz reservoir, northern Spain, in Poromechanics-iv, edited by H. Ling, A. Smyth and R.Betti, Destech Publications, Inc., Lancaster, Pennsylvania, ISBN: 978-1-60595-006-8, 1109– 1114.

Luzón, F., García-Jerez, A., Santoyo, M. A., and Sánchez-Sesma, F. J. (2010), Numerical modelling of pore pressure variations due to time varying loads using a hybrid technique: the case of the Itoiz reservoir (Northern Spain), *Geophys. J. Int*., 180, 327–338, doi: 10.1111/j.1365-246X.2009.04408.x.

Madariaga, R. (1976), Dynamics of an Expanding Circular Fault, *Bull. Seism Soc. Am.,* 66**,** 639–666.

Mai, P.M. and Beroza, G.C. (2000), Source scaling properties from finite-fault rupture models. Bull. Seism. Soc. Am., 90, 604–615.

Mandal, P., Rastogi, B.K. and Sarma, C.S.P. (1998), Source parameters of Koyna earthquakes, India, *Bull. seism. Soc. Am.,* 88**,** 833–842.

This is a post-peer-review, pre-copyedit version of an article published in Pure and Applied Geophysics. The final authenticated version is available online at: http://dx.doi.org/10.1007/s00024-014-0883-y

Maurer, W., Dowla, F. and Jarpe, S. (1992), Seismic event interpretation using self-organizing neural networks, in *Proceedings of the International Society for Optical Engineering (SPIE),* Vol. 1709, 950–958, doi:10.1117/12.139971.

Michalewicz, Z. (1992). Genetic Algorithms + Data Structures = Evolution Programs, *Springer-Verlag, Berlin Heidelberg*.

Mori, J., and Frankel, A. (1990), Source parameters for small events associated with the 1986 north Palm Springs, California, earthquakes determined using empirical Green's functions, *Bull. Seism. Soc. Am.* 80**,** 278–295.

Moya, A., Aguirre J. and Irikura, K. (2000), Inversion of source parameters and site effects from strong ground motion records using genetic algorithms. *Bull. Seism. Soc. Am*., 90, 977–992.

Musil, M. and Plešinger, A. (1996), Discrimination between local microearthquakes and quarry blasts by multi-layer perceptrons and Kohonen maps, *Bull. Seism. Soc. Am.*, 86(4), 1077–1090.

Oncescu, M.C., Camelbeeck, T. and Martin, H. (1994), Source parameters for the Roermond aftershocks of April 13 - May 2, 1992 and site spectra for P and S waves at the Belgian seismic network, *Geophys. J. Inter*. 116, 673-682.

Ozerdem, M. S., Ustundag, B. and Demirer, R. M. (2006), Self-organized maps based neural networks for detection of possible earthquake precursory electric field patterns, Advances in Engineering Software 37 (4), 207-217, doi: 10.1016/j.advengsoft.2005.07.004.

Pedreira D., Pulgar, J. A. Gallart, J. and Díaz, J. (2003), Seismic evidence of Alpine crustal thickening and wedging from the western Pyrenees to the Cantabrian Mountains (north Iberia), *J. Geophys. Res*., 108 (B4), 2204, doi:10.1029/2001JB001667.

This is a post-peer-review, pre-copyedit version of an article published in Pure and Applied Geophysics. The final authenticated version is available online at: http://dx.doi.org/10.1007/s00024-014-0883-y

Plešinger, A., Růžek, B. and Boušková, A. (2000), Statistical interpretation of WEBNET seismograms by artificial neural nets, *Studia Geophysica et Geodaetica,* 44(2), 251–271, doi: 10.1023/A:1022119011057.

Prejean, S. G., and Ellsworth, W. L. (2001), Observations of earthquake source parameters at 2 km depth in the Long Valley Caldera, Eastern California, *Bull. Seism. Soc. Am.* 91**,** 165–177.

Pujades, L. G., Canas, J. A. Egozcue, J. J. Puigvi, M. A. Gallart, J. Lana, X. Pous, J. and Casas, A. (1990), Coda *Q* distribution in the Iberian Peninsula, *Geophys. J. Int.* 100**,** 285–301.

Reeves, C. (1993). Modern Heuristic Techniques for Combinatorial Problems, *Blackwell Scientific Publications*.

Rivas-Medina, A., Santoyo, M. A. Luzón, F. Benito, B. Gaspar-Escribano, J. M. and García-Jerez, A. (2011), Seismic Hazard and ground motion characterization at the Itoiz dam (Northern Spain), Pure Appl. Geophys., doi: 10.1007/s00024-011-0405-0.

Ruiz, M., Gaspa, O. Gallart, J. Díaz, J. Pulgar, J. A. García-Sansegundo, J. López-Fernández, and C. González-Cortina, J. M. (2006), Aftershocks series monitoring of the September 18, 2004 3 M =4.6 earthquake at the western Pyrenees: A case of reservoir triggered seismicity?, *Tectonophysics*, 424, 223–243, doi: 10.1016/j.tecto.2006.03.037.

Santoyo, M. A., García-Jerez, A. and Luzón, F. (2010), A subsurface stress analysis and its possible relation with seismicity near the Itoiz Reservoir, Navarra, Northern Spain, *Tectonophysics*, 482, 205–215, doi: 10.1016/j.tecto.2009.06.022.

Sato, T., and Hirasawa, T. (1973), Body wave spectra from propagating shear cracks, *J. Phys. Earth*, 21, 415-431.

This is a post-peer-review, pre-copyedit version of an article published in Pure and Applied Geophysics. The final authenticated version is available online at: http://dx.doi.org/10.1007/s00024-014-0883-y

Scholz, C.H. (1990), *The mechanics of earthquakes and faulting*. Cambridge University Press, Cambridge.

Shieh, C. F (1995), Study on the free surface coupling effect of seismic waves. *TAO*, 6, 197-207.

Smith, K.D., and Priestley, K.F. (1993), Aftershocks stress release along active fault planes of the 1984 Round Valley, California, earthquake sequence applying time – domain stress drop method, *Bull. Seism. Soc. Am*., 83, 144-159.

Snoke, J. A. (1987), Stable determination of (Brune) stress drops, *Bull. Seism. Soc. Am.* 77, 530-538.

Steidl, J. H., Tumarkin, A. G. and Archuleta, R. J. (1996), What is a reference site?, *Bull. Seism. Soc. Am.*, 86, 1733-1748.

Tarvainen, M. (1999), Recognizing explosion sites with a self-organizing network for unsupervised learning, *Phys. Earth planet. Int.*, 113(1–4), 143–154.

Tomic, J., Abercrombie R. E. and do Nascimento, A. F. (2009), Source parameters and rupture velocity of small $M \leq 2.1$ reservoir induced earthquakes *Geophys. J. Int.*, 179**,** 1013–1023 doi: 10.1111/j.1365-246X.2009.04233.x.

Tusa, G. and Gresta, S. (2008), Frequency-Dependent Attenuation of P Waves and Estimation of Earthquake Source Parameters in Southeastern Sicily, Italy, *Bull. Seism. Soc. Am.*, 98 (6), 2772–2794, doi: 10.1785/0120080105.

Zelt, B. C., Dotzev, N.T. Ellis, R.M. and Rogers, G.C. (1999), Coda Q in Southwestern Columbia, Canada, *Bull. Seism. Soc. Am.*, 89, 1083-1093.

This is a post-peer-review, pre-copyedit version of an article published in Pure and Applied Geophysics. The final authenticated version is available online at: http://dx.doi.org/10.1007/s00024-014-0883-y

Table 1. Source parameters of the analyzed events. EM, Er, and Es are the multiplicative errors in moment, radius and stress drop, respectively.

nsis	date	magnitude (mbLg)	Moment (Nm)	radius (km)	stress drop (MPa)	EM	Er	Es	number of stations
1	20040916191706	3.2	8.65E+13	0.31	1.217	5.06	2.38	32.77	3
2	20040917025856	3	7.43E+12	0.21	0.346	2.47	3.08	11.82	2
3	20040918125218	5.2	2.65E+15	0.34	29.462	2.19	1.48	1.54	3
4	20040918125507	3.2	1.98E+14	0.24	6.532	-	-	-	1
5	20040918152547	2.5	1.54E+13	0.73	0.018	-	-	-	1
6	20040918195828	3.1	2.60E+13	1.00	0.011	-	-	-	1
7	20040919054023	2.8	6.73E+13	0.27	1.440	-	-	-	1
8	20040930130907	3.9	1.90E+14	0.38	1.506	1.73	2.81	15.09	3
9	20041007061630	3.4	4.55E+13	0.46	0.207	3.73	2.01	12.97	3
10	20041020164719	2.7	3.31E+13	0.34	0.355	1.76	2.27	17.48	3
11	20041023174246	2.9	1.34E+13	0.31	0.189	6.15	1.80	35.93	3
12	20041109112619	2.9	9.75E+12	0.27	0.218	2.14	2.88	11.13	2
13	20060111031417	1.5	1.72E+11	0.19	0.012	-	-	-	1
14	20060111033502	1.2	1.80E+11	0.14	0.030	-	-	-	1
15	20060111142103	1.5	4.64E+11	0.09	0.305	-	-	-	1
16	20060111143211	1.4	2.39E+11	0.12	0.066	-	-	-	1

This is a post-peer-review, pre-copyedit version of an article published in Pure and Applied Geophysics. The final authenticated version is available online at: http://dx.doi.org/10.1007/s00024-014-0883-y

17	20060111184704	1.6	2.04E+11	0.16	0.021	-	-	-	1
18	20070411014540	2.9	1.51E+13	0.36	0.141	4.42	1.69	2.18	3
19	20070514125550	2.3	3.74E+12	0.17	0.342	-	-	-	1
20	20070608123322	1.9	7.94E+11	0.10	0.321	-	-	-	1
21	20070731214029	2.7	3.45E+12	0.47	0.015	1.87	1.54	6.87	2
22	20070829075318	3.1	1.39E+13	0.34	0.151	1.91	1.91	5.25	4
23	20071015205657	2.8	5.31E+12	0.20	0.306	2.69	2.10	8.56	5
24	20071122112044	2.3	3.51E+12	0.29	0.065	1.23	1.99	6.49	3
25	20071122185450	2.1	1.56E+12	0.44	0.008	2.17	1.78	3.71	3
26	20080426135505	2.8	7.40E+12	0.33	0.093	2.32	1.57	3.89	4
27	20080517041011	2.3	2.21E+12	0.32	0.030	3.12	1.51	3.54	4
28	20080526160213	2.6	2.37E+13	0.34	0.258	5.67	1.38	2.17	2
29	20080604210825	2.9	1.78E+13	0.32	0.234	1.45	1.35	1.70	2
30	20080622074755	2.4	3.29E+12	0.32	0.042	-	-	-	1
31	20080625010713	2.1	7.12E+11	0.27	0.016	3.27	1.89	4.41	4
32	20080627195904	2	4.36E+11	0.32	0.006	-	-	-	1
33	20080709082814	2	1.99E+12	0.21	0.093	1.82	1.25	3.58	2
34	20080725212446	2.7	1.41E+13	0.46	0.065	4.26	2.88	8.18	4
35	20080915041001	2.4	1.86E+12	0.15	0.234	1.13	1.41	2.48	2
36	20080916070024	2.8	4.91E+12	0.32	0.065	1.33	1.89	7.78	4
37	20080920161022	2.4	2.98E+12	0.22	0.124	1.46	1.49	4.63	3
38	20080928135600	2.4	1.47E+12	0.31	0.022	1.90	1.12	2.29	3
39	20081010133108	2.9	8.43E+12	0.19	0.516	1.94	2.27	11.67	5
40	20081126063000	2.2	2.95E+12	0.20	0.162	1.58	1.51	2.35	3
41	20081211210757	2.8	4.62E+13	0.28	0.950	2.12	1.31	1.77	4
42	20090121200701	2.9	1.18E+14	0.42	0.700	2.06	1.61	3.18	8
43	20090127212208	2.5	5.46E+13	0.73	0.063	-	-	-	1
44	20090701150326	2.6	1.02E+14	0.33	1.200	1.43	1.05	1.25	2
45	20091024200524	2.6	2.41E+13	0.33	0.282	1.08	1.43	3.12	2

This is a post-peer-review, pre-copyedit version of an article published in Pure and Applied Geophysics. The final authenticated version is available online at: http://dx.doi.org/10.1007/s00024-014-0883-y

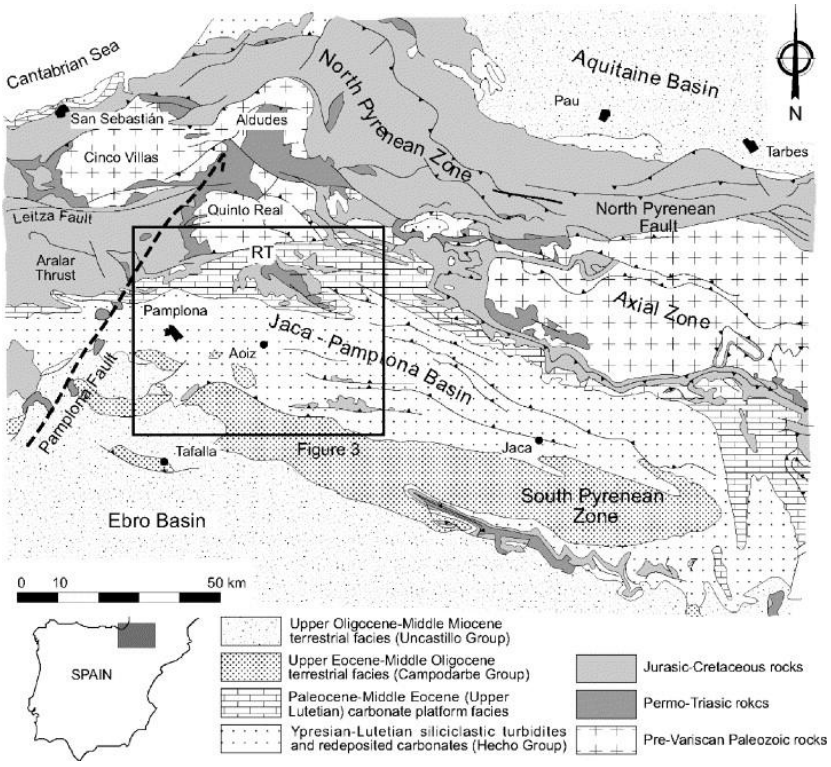

Figure 1. Geological setting (Ruiz et l., 2006).

This is a post-peer-review, pre-copyedit version of an article published in Pure and Applied Geophysics. The final authenticated version is available online at: http://dx.doi.org/10.1007/s00024-014-0883-y

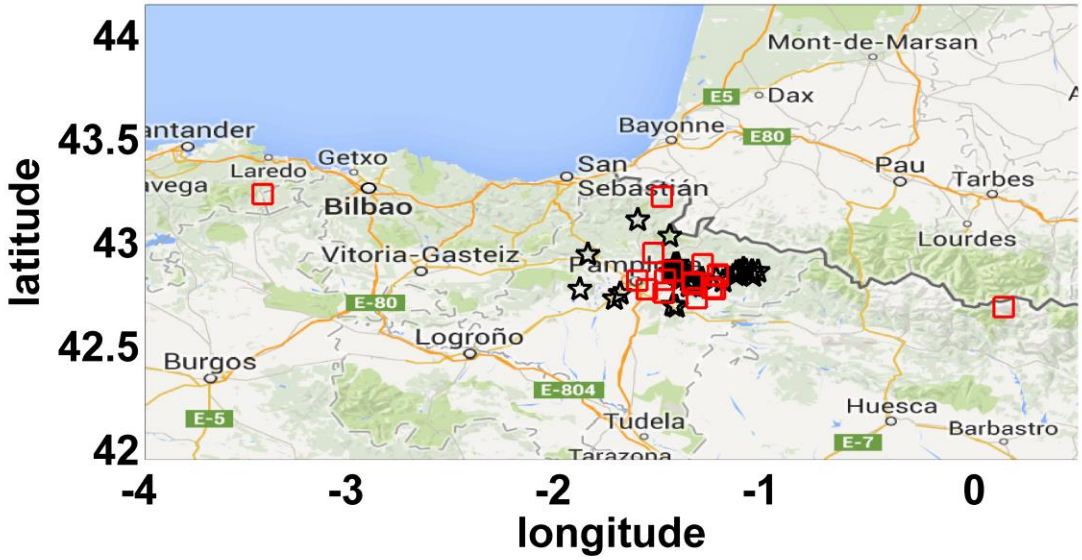

Figure 2. Location of the analyzed events (stars) and the stations (red squares).

This is a post-peer-review, pre-copyedit version of an article published in Pure and Applied Geophysics. The final authenticated version is available online at: http://dx.doi.org/10.1007/s00024-014-0883-y

1

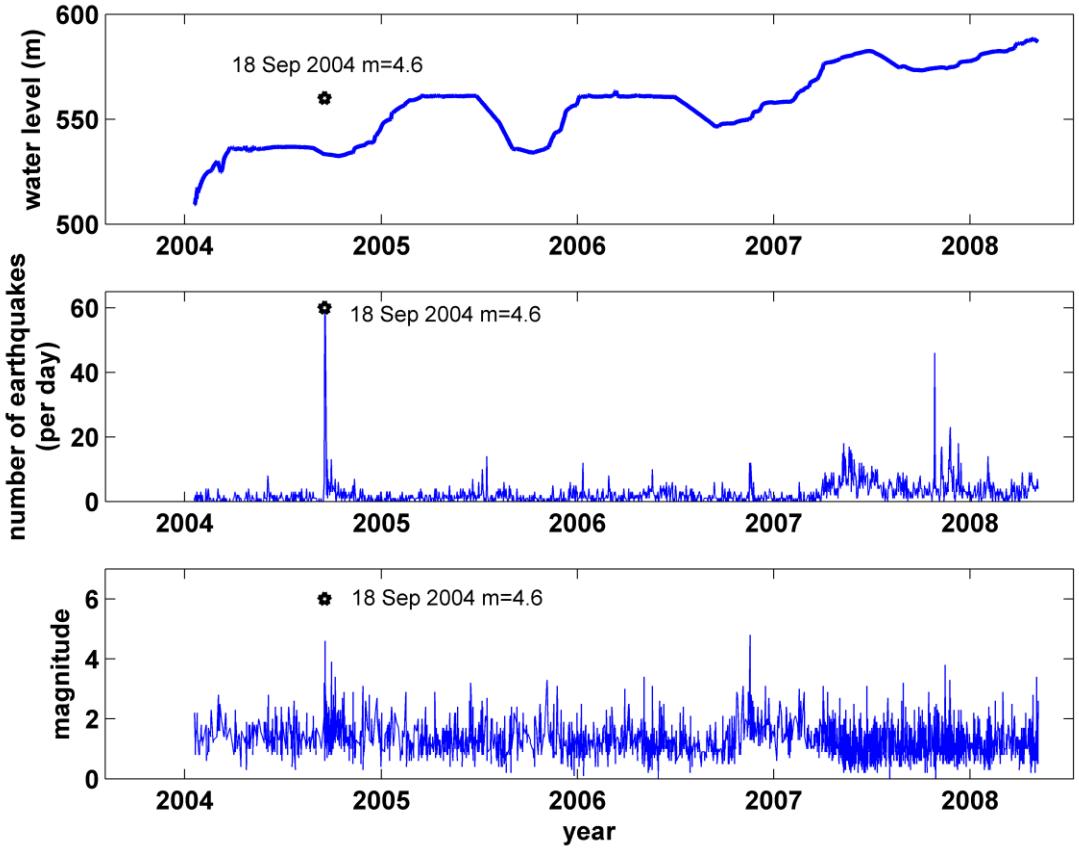

2

3 Figure 3. Water level and seismicity near the Itoiz dam over time.

4

5

6

7

8

9

10

11

12

This is a post-peer-review, pre-copyedit version of an article published in Pure and Applied Geophysics. The final authenticated version is available online at: http://dx.doi.org/10.1007/s00024-014-0883-y

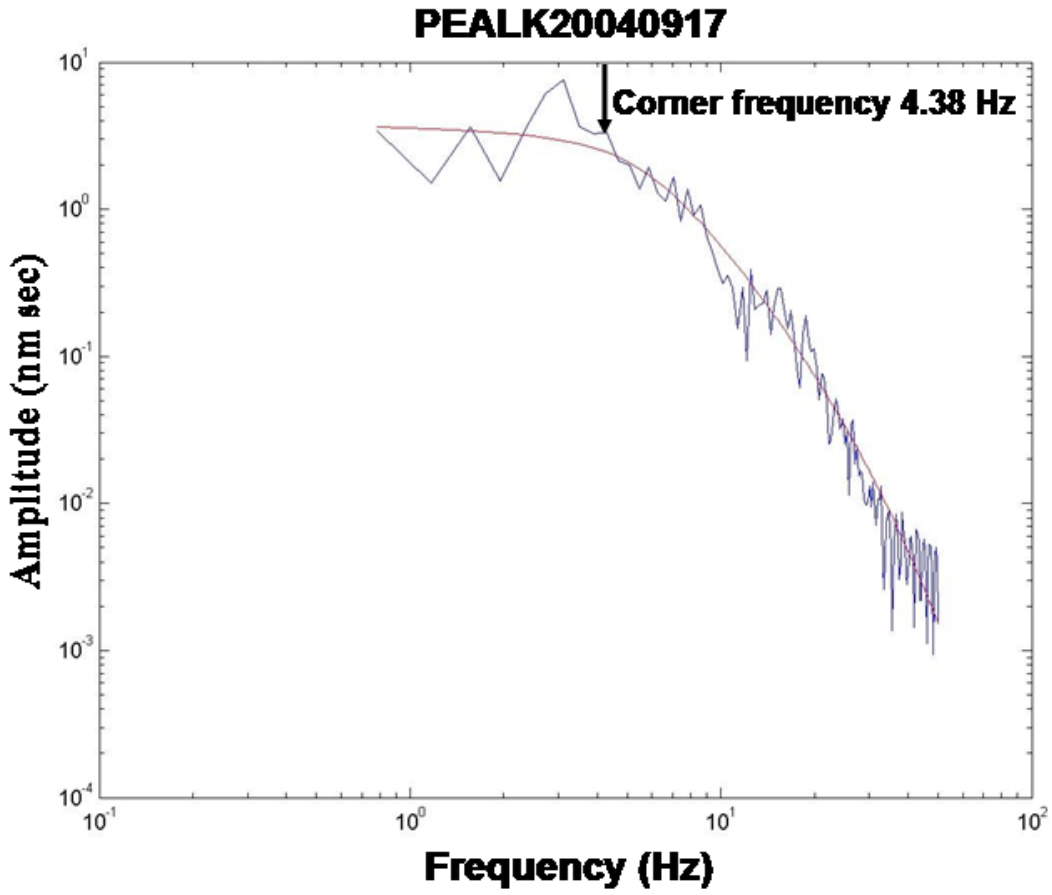

Figure 4. Example of fitted spectrum. In red the fitted spectrum, and in blue the real one. The corner frequency is plotted too.

This is a post-peer-review, pre-copyedit version of an article published in Pure and Applied Geophysics. The final authenticated version is available online at: http://dx.doi.org/10.1007/s00024-014-0883-y

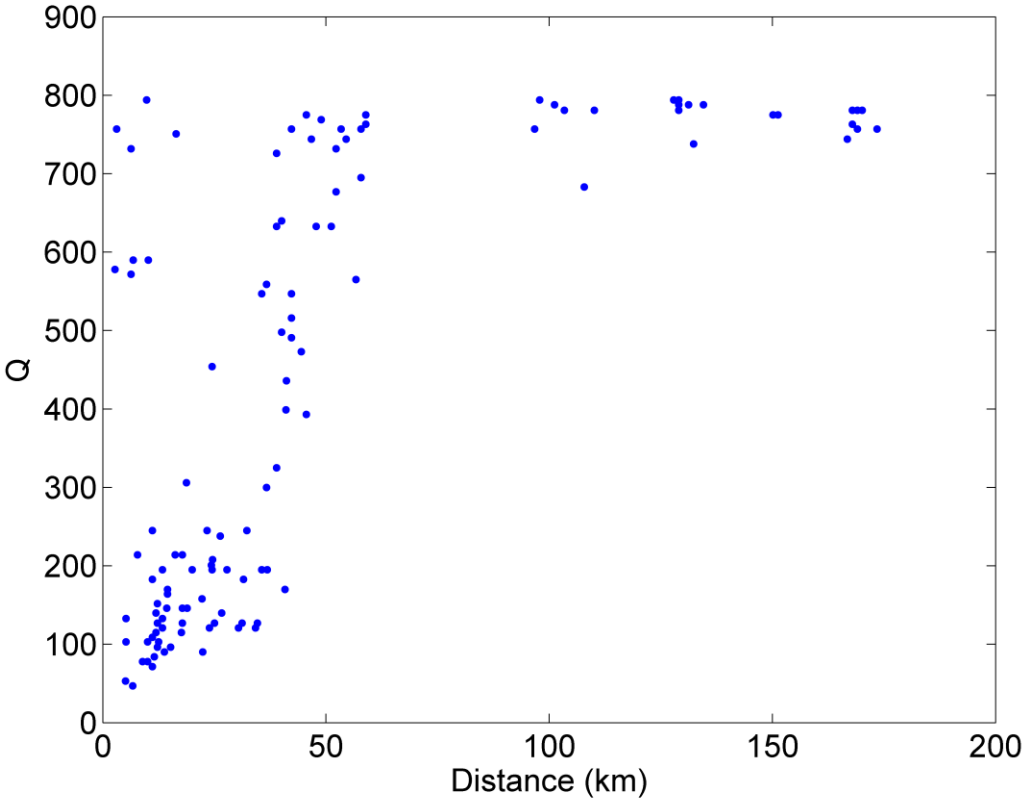

Figure 5. Attenuation factors vs. distance between event and station. Each point represents only one path.

This is a post-peer-review, pre-copyedit version of an article published in Pure and Applied Geophysics. The final authenticated version is available online at: http://dx.doi.org/10.1007/s00024-014-0883-y

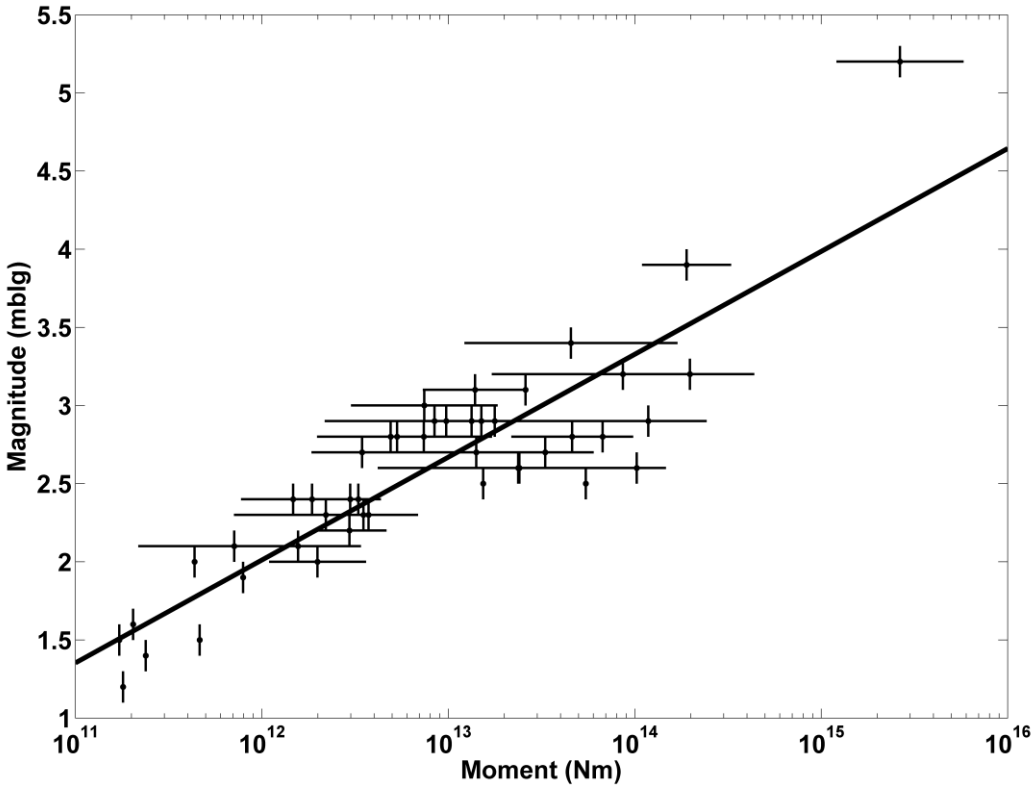

Figure 6. Relationship between magnitude and moment, with their corresponding errors. We also plot the line which best fits the data. The dots with only vertical error bars were obtained by analyzing just one spectrum.

This is a post-peer-review, pre-copyedit version of an article published in Pure and Applied Geophysics. The final authenticated version is available online at: http://dx.doi.org/10.1007/s00024-014-0883-y

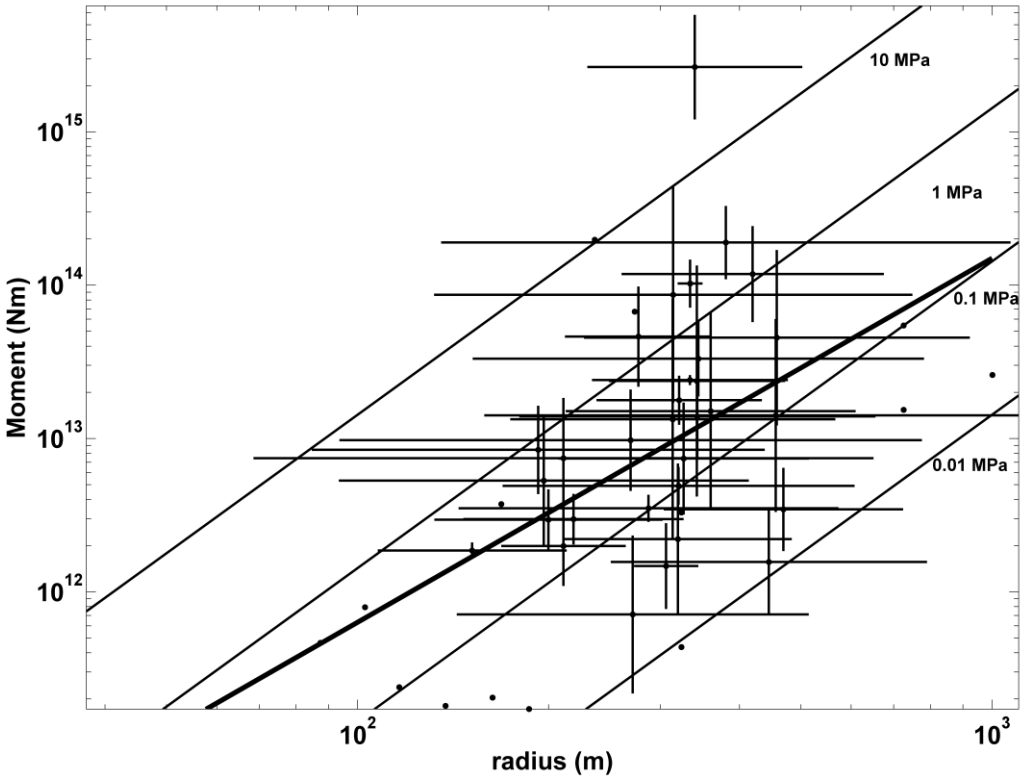

Figure 7. Radius vs. moment with their errors bars. The lines are contours of equal stress drops in MPa. The best fit is also presented, with a thicker line. The dots with no error bars were obtained by analyzing just one spectrum.

This is a post-peer-review, pre-copyedit version of an article published in Pure and Applied Geophysics. The final authenticated version is available online at: http://dx.doi.org/10.1007/s00024-014-0883-y

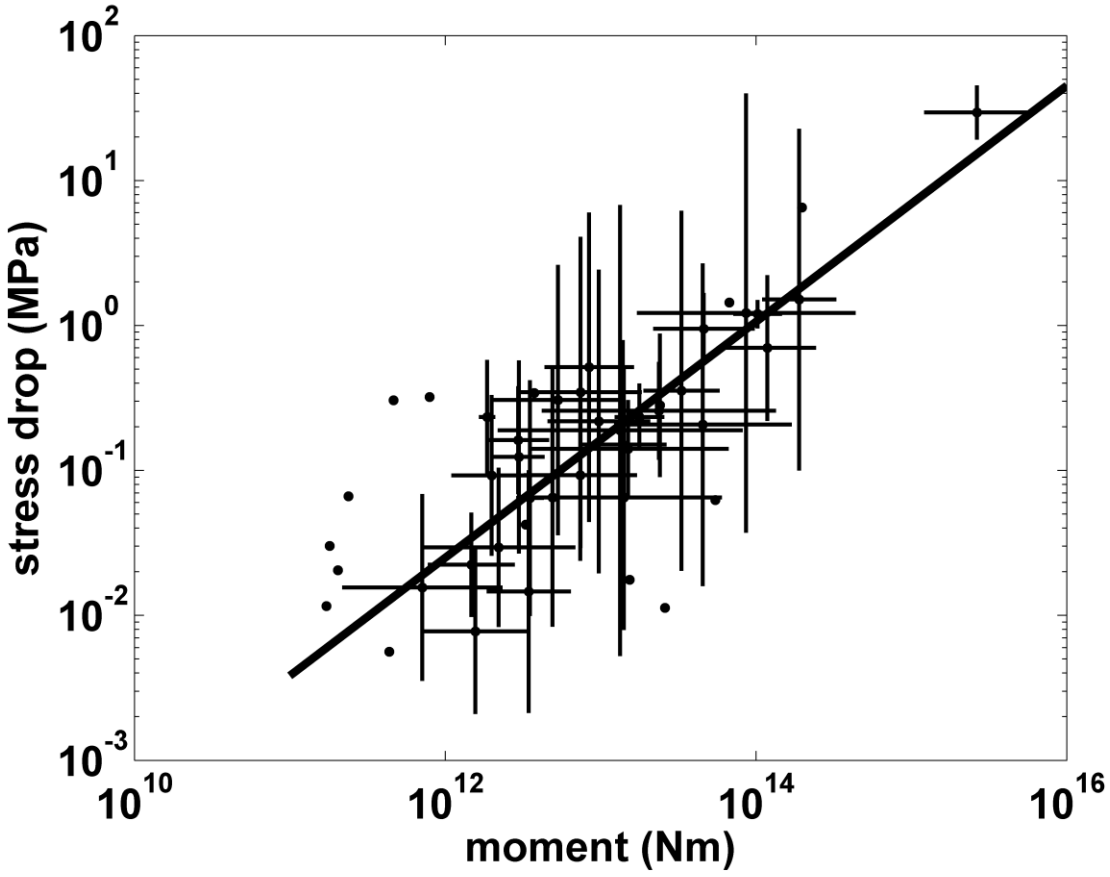

Figure 8. Moment vs. stress drop, with the corresponding error bars. The line is the best fit, without including the data with only one or two records. The dots with no error bars were obtained by analyzing just one spectrum.

This is a post-peer-review, pre-copyedit version of an article published in Pure and Applied Geophysics. The final authenticated version is available online at: http://dx.doi.org/10.1007/s00024-014-0883-y

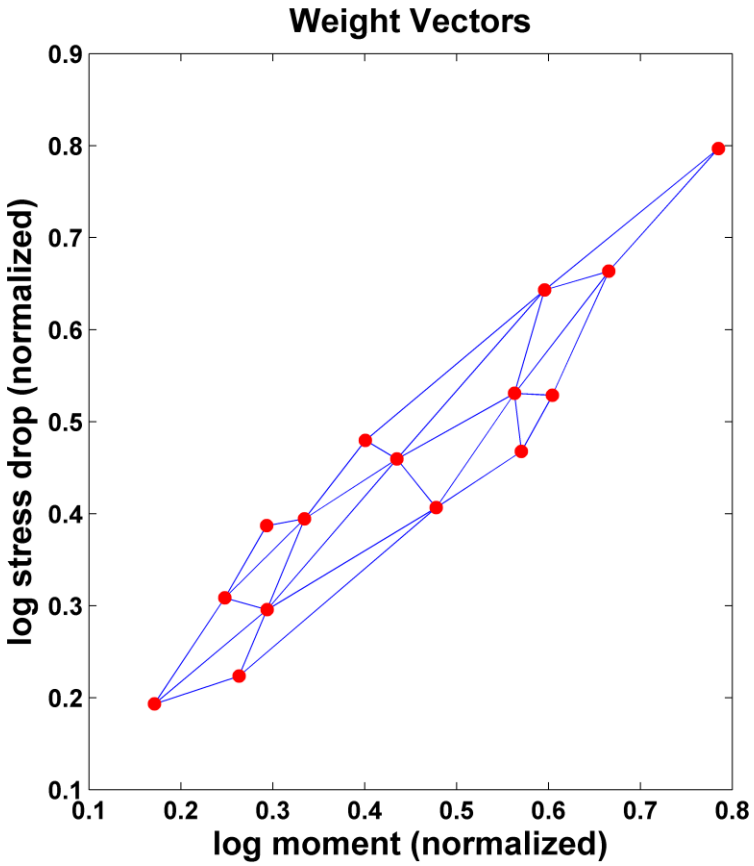

Figure 9. Results of the SOM algorithm to the data in the Granada basin. In the x axis we represent the rescaled logarithm (in base 10) of the moment from 0 to 1, and in the y axis the rescaled logarithm of the stress drop.

This is a post-peer-review, pre-copyedit version of an article published in Pure and Applied Geophysics. The final authenticated version is available online at: http://dx.doi.org/10.1007/s00024-014-0883-y

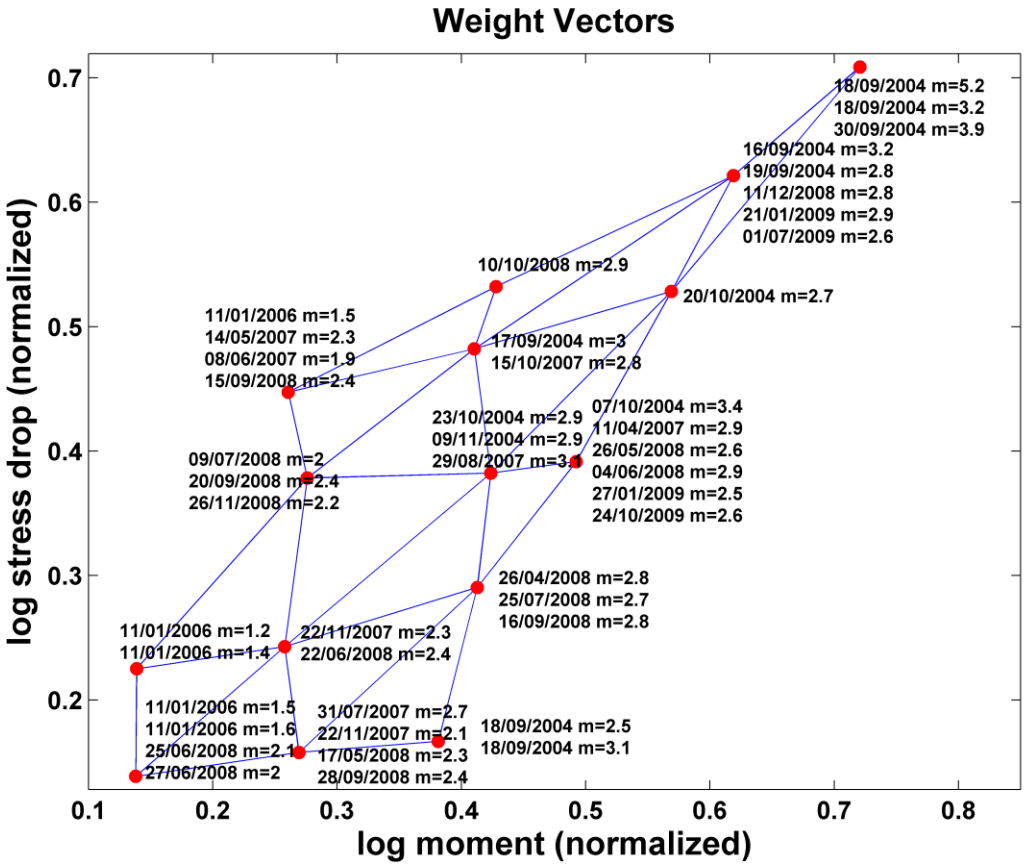

Figure 10. Results of the SOM algorithm to the data in the Itoiz dam. In the x axis we represent the rescaled logarithm (in base 10) of the moment from 0 to 1, and in the y axis the rescaled logarithm of the stress drop.

This is a post-peer-review, pre-copyedit version of an article published in Pure and Applied Geophysics. The final authenticated version is available online at: http://dx.doi.org/10.1007/s00024-014-0883-y

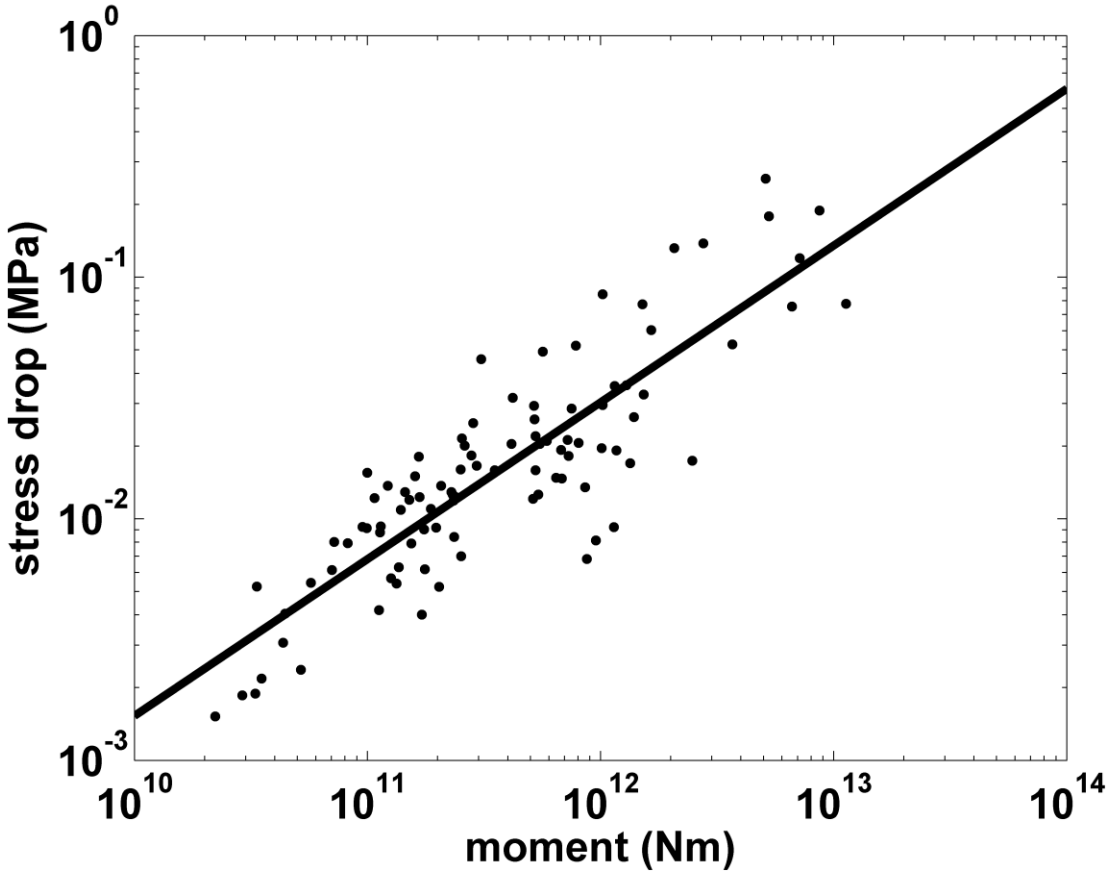

Figure 11. Moment vs. stress drop, for the data in García et al. (1996). The line is the best fit.

This is a post-peer-review, pre-copyedit version of an article published in Pure and Applied Geophysics. The final authenticated version is available online at: http://dx.doi.org/10.1007/s00024-014-0883-y